COMBUSTION SCIENCE AND TECHNOLOGY
2024, VOL. 196, NO. 14, 2356–2379
https://doi.org/10.1080/00102202.2022.2135995

Taylor & Francis
Taylor & Francis Group

Influence of Pyrolysis Gas Composition and Reaction Kinetics on Leaf-Scale Fires

Peyman Rahimi Borujerdi[a], Babak Shotorban[a], Shankar Mahalingam[a], and David R. Weise[b]

[a]Department of Mechanical and Aerospace Engineering, The University of Alabama in Huntsville, Huntsville, AL, USA; [b]Pacific Southwest Research Station, USDA Forest Service, Riverside, CA, USA

ABSTRACT

The impact of pyrolysis gas composition and the underlying reaction kinetics on the burning characteristics of a leaf was computationally investigated. The computational configuration resembled a previous experimental setup where vertically oriented manzanita (*Arctostaphylos glandulosa*) leaves were burned. Different compositions and reaction kinetics for the pyrolysis gas released during the leaf thermal decomposition were examined. The most detailed composition included CH_4, CO, CO_2, and H_2, which was suggested by the previous experimental study of pyrolysis products of different plant species. The least involved compositions only included either CH_4 or CO. In all considered compositions, in addition to pyrolysis gas, the release of the heavy gas, i.e. tar, was accounted for. Tar breakdown was represented by a single-step reaction with the light gases above and soot as the products where the stoichiometric coefficients were determined by an optimization technique for consistency with the measurements for the tar molecule. The burning simulation results agreed best with the previous experimental data when a mixture of CH_4, CO, CO_2 was used. The least agreement was noted when pyrolysis gas was represented by only CH_4. Inclusion of tar breakdown reaction appreciably increased the overall heat release due to combustion of its products above the leaf.

ARTICLE HISTORY
Received 8 June 2021
Revised 23 August 2022
Accepted 8 September 2022

KEYWORDS
Pyrolysis; reaction kinetics; combustion; tar; live fuel

1. Introduction

Combustion of the pyrolysis gas released from a thermally degrading wildland fuel plays a critical role in wildfire spread mainly by supplying heat to both burning and unburned fuel particles. In fact, the pyrolysis gas is a complex and highly variable mixture of gaseous species (Zhou and Mahalingam 2001). Volatile gases, in general, are comprised of non-condensable light gases, such as CO, CO_2, and H_2, light hydrocarbons, such as CH_4, C_2H_4, and C_3H_8, and heavy condensable gases called tar (Di Blasi 2008; Lee et al. 2007; Leroy et al. 2008; Tihay et al. 2009; Safdari et al. 2018).

This motivated the study here as to how the model predictions are affected by the assumed composition of the pyrolysis products and the corresponding reaction mechanism describing their chemical evolution.

CONTACT Babak Shotorban babak.shotorban@uah.edu The University of Alabama in Huntsville, 301 Sparkman Dr. NW, Huntsville, AL 35899, USA

Different approaches to model pyrolysis gas combustion have been proposed. A straightforward method is to represent the combustible part of the pyrolysis gas with only one fuel species. Considering the fact that carbon monoxide constitutes a considerable part of the pyrolysis gas (Boroson et al. 1989; Wagenaar et al. 1993; Tihay et al. 2009; Safdari et al. 2018), in some works (Grishin 1997; Morvan and Dupuy 2001; Morvan et al. 2004; Zhou et al. 2005) the combustion of volatile gases was modeled by a single reaction for CO oxidation. Some others (Yashwanth et al. 2016; Shotorban et al. 2018; Borujerdi et al. 2020) used methane in lieu of carbon monoxide. In two studies (Ritchie et al. 1997; Mell et al. 2009a), the fuel was represented by a single but more involved species in the form of an oxygenated hydrocarbon as $C_{3.4}H_{6.2}O_{2.5}$. This was partly motivated by the fact that hydrocarbon compounds in the form of oxygenated hydrocarbons were observed in the biomass pyrolysis products (Ni et al. 2006).

In addition to one-step reaction kinetics models reviewed above, more advanced schemes in the form of multi-step global, reduced, and skeletal mechanisms have been used to model combustion of pyrolysis gases (Zhou and Mahalingam 2001; Leroy et al. 2008; Tihay et al. 2009). Zhou and Mahalingam (2001) assumed that the pyrolysis gas consists of CH_4, CO, CO_2, and H_2 and developed a reduced mechanism for combustion of this mixture. First, they derived a skeletal mechanism from GRI-Mech 3.0 (Smith et al. 2000) and then using steady-state and partial equilibrium assumptions (Turns 1996), they obtained the reduced mechanism from the skeletal mechanism. This reduced scheme was validated in three different settings. Furthermore, the impact of mixture composition on the flame temperature and speed was investigated. It was noted that when the concentration of CO and H_2 was smaller, flame temperature was lower. Leroy et al. (2008) performed experiments on the burning of *Pinus Pinaster*, a common Mediterranean plant species. They noted that the pyrolysis products were mainly composed of CH_4, CO, and CO_2. They proposed both skeletal and reduced reaction mechanisms for combustion of this mixture. These mechanisms were tested against the experiments with a relative success, showing an overall good agreement between experimental and simulated species concentration profiles. Tihay et al. (2009) experimentally burned samples of six common Mediterranean plant species. They determined the composition of gases released during the thermal decomposition of these samples. They observed that for all samples, CO_2 was the dominant gaseous species followed by CO and H_2O. Tihay et al. (2009) simulated the burning experiments using four skeletal mechanisms and concluded that the one proposed by Peters and Kee (1987) performed better in terms of the computational cost and agreement with the experimental data.

Tihay et al. (2009) also examined three global mechanisms. Using global mechanisms is advantageous with respect to the computational time (Tihay et al. 2009). The first mechanism only included CO oxidation reaction and its reverse reaction. In addition to this, the second mechanism included the one-step reaction of stoichiometric CH_4 complete combustion. The third mechanism was similar to the second one, except for the fact that the one-step reaction of CH_4 was incomplete, including CO in the products. The effect of the pyrolysis gas composition was also investigated in this work. Tihay et al. (2009) observed that when CH_4 was not present in the combustion model, the comparison between numerical and experimental data was not satisfactory. On the other hand, the results of the third mechanism matched reasonably well with the experimental data for temperature.

In the present work, the effects of pyrolysis gas composition and the corresponding reaction mechanism on the burning of a leaf-like fuel were investigated. The work presented here was in part motivated by the experimental findings of Safdari et al. (2018) where 14 plant species (dead and live) were heated by flow of hot gases exiting a flat flame burner (FFB) and without any oxidizing agent to prevent flaming combustion. The temperature of hot gases near the sample in the FFB was measured and reported to be $\sim 765^{\circ}$C. Pyrolysis products were analyzed, and it was shown that the composition of the pyrolysis products of a specific plant did not change appreciably between dead and live states. Also, it was observed that the condensable heavy gas, i.e. tar, had the highest mass yield among all gaseous species in the volatile gas mixture. More importantly, it was noted that, for all plant species, CO, CO_2, CH_4, and H_2 were the components of the light gas. Safdari et al. (2018) averaged the yield of these four gases over 14 plant species and presented an average light gas composition. Guided by this finding, several compositions were examined here. Furthermore, since tar was shown to have a large yield, the influence of tar breakdown considered as a secondary pyrolysis was also investigated.

2. Computational model

In this work, Gpyro3D (Lautenberger 2014) modified (Shotorban et al. 2018) and coupled with Fire Dynamic Simulator (FDS) (McGrattan et al. 2013) was utilized for simulations. Representing the thermal decomposition of the leaf, Gpyro3D numerically solves a set of partial differential equations describing the thermochemical and physical processes a porous solid fuel undergoes when subject to heating. On the other hand, FDS solves the low Mach number form of conservation equations for mass, momentum, energy, and chemical species in the gas phase surrounding the solid fuel. Here, FDS is set to run in the Direct Numerical Simulation (DNS) mode. When FDS is run in the DNS mode, convective heat flux on a solid surface is directly calculated from difference between the solid surface temperature and the temperature of the gas in the adjacent computational cell. The effect of soot formation and transport is neglected. Radiative heat transfer is dealt with by the solution of radiation transport equation (RTE) for the gray gas. To solve the RTE, a finite volume method with approximately 100 discrete angles is used. The absorption coefficient of the gas mixture is calculated as the summation over individual gases' gray of band-mean absorption coefficient (McGrattan et al. 2013). Gray absorption coefficient of an individual gas is evaluated by RADCAL approach (Grosshandler 1993). Gpyro3D and FDS are coupled by imposing the continuity of temperature, mass fractions, and heat and mass fluxes at the interface of Gpyro3D and FDS domains (Yashwanth et al. 2016).

Shown in Figure 1 is the computational setup used in the simulations. It resembles the experimental setup of Prince (2014) where manzanita (*Arctostaphylos glandulosa*) leaves were burned by means of convective heating. In each burning experiment, the leaf was positioned in a glass duct so that its longest dimension had a vertical orientation. It is noted that the leaves of a manzanita stand have a tendency for the vertical orientation (Wilken 1967). Convective heating was supplied by a flat flame burner (FFB) which was rolled into a position directly under the leaf. The exhaust gases of the FFB were measured undefined°C and 10 mol% oxygen prince (Prince 2014).

The computational setup dimensions are $0.18 \times 0.25 \times 0.32$ m ($x \times y \times z$). Leaf faces are parallel to FFB convection streams thereby inducing the formation of boundary layers

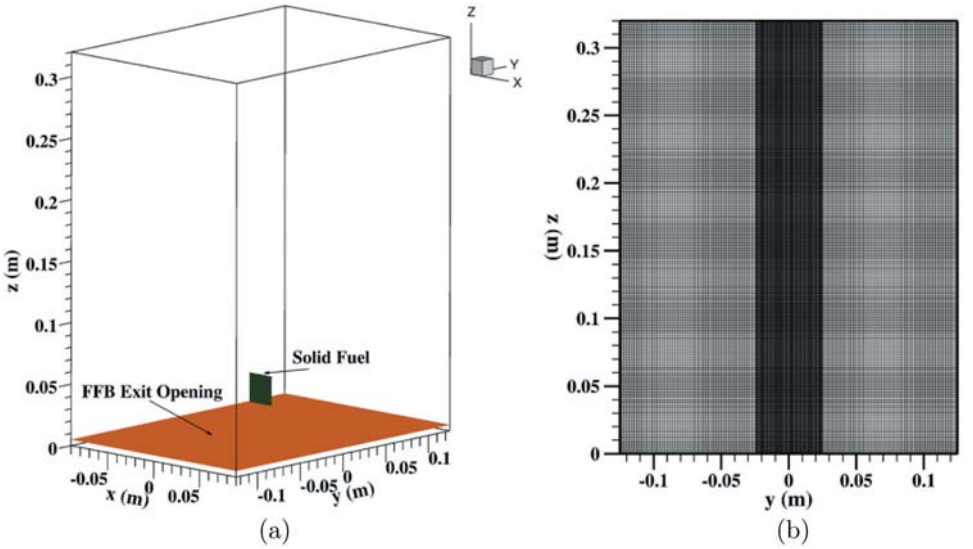

Figure 1. (a) Isometric view of the computational domain displaying the vertically oriented solid fuel held over an FFB, and (b) a two-dimensional view of the computational mesh on the *yz* plane showing the nonuniformity of the mesh with finer grids in the central zone.

on the leaf faces. Consequently, a nonuniform mesh in the gas-phase domain with a finer resolution near the faces was used. The central zone of the domain, which included leaves and extended from $y = \quad 0.025$ m to $y = 0.025$ m, was resolved with a grid resolution of 120 $\times$ 99 $\times$ 216 (cell size of 1.50 $\times$ 0.51 $\times$ 1.48 mm) in x, y and z directions, respectively. The rest of the domain has a coarser grid resolution of 120 $\times$ 132 $\times$ 216 (cell size of 1.50 $\times$ 1.51 $\times$ 1.48 mm).

The manzanita leaf is represented by a thin rectangular solid object centered 4 cm above the bottom surface of the domain. Modeled leaf dimensions are 23.7 $\times$ 0.51 $\times$ 23.7 mm ($x \times y \times z$). A uniform mesh with a grid resolution of 48 $\times$ 6 $\times$ 48 in x, y and z directions is used for the leaf in the Gpyro3D domain. Sufficiency of the grid resolutions in both FDS and Gpyro3D domains have been demonstrated previously (Borujerdi et al. 2020; Borujerdi and Shotorban (2022). Also, it is noted that the overall energy transfer from the gas to the solid fuel changed by only about 3% when the cell size in the FDS was doubled in x and z directions. As a result of the chosen dimensions, the surface area is computed 5.62 cm^2 which is identical to the mean measured area reported for manzanita leaves (Pickett et al. 2010). Dry-basis fuel moisture content (FMC) is 63% as reported in the experiments for a fresh live leaf (Prince 2014). With this moisture content, the initial solid fuel mass in simulations is set to 0.2156 g. This value is within the range of measured mass 0.2197 $\pm$ 0.0127 g reported for manzanita leaves with FMCs in the range of 44% to 107% (Pickett et al. 2010). The initial composition of the leaf dry mass is set to 33 wt% cellulose, 33 wt% hemicellulose, and 34 wt% lignin (Sheng and Azevedo 2002; Pickett 2008; Prince 2014). Assuming that the dry mass of the leaf only consists of cellulose, hemicellulose, and lignin will allow the use of a previously validated biomass pyrolysis model described later in this section. A recent experimental investigation of live leaves from several forest plants, excluding manzanita, revealed that while cellulose,

Table 1. Thermophysical properties of the moist fuel constituents (Shotorban et al. 2018). Here, ρ is apparent density, $\hat{\rho}$ true density, k thermal conductivity, and c specific heat capacity. Dry fuel is regarded to any of the species cellulose, hemicellulose, and lignin, assumed to have identical thermophysical properties Miller and Bellan (1997).

Species	ρ (kg/m^3)	$\hat{\rho}$ (kg/m^3)	k (W/mK)	c (kJ/kgK)	Reference
Moisture	-	1000	0.596	3.9	Bryden et al. (2002)
Dry fuel	650	2167	0.1256	2.3	Miller and Bellan (1997)
Char	350	2333	0.0837	1.1	Miller and Bellan (1997)

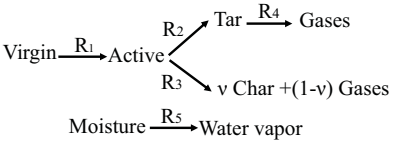

Figure 2. Generic reaction mechanism for moist fuel (Shotorban et al. 2018) involving pyrolysis of dry fuel constituents, viz. cellulose, hemicellulose and lignin at virgin states (Miller and Bellan 1997), and moisture evaporation (Bryden and Hagge 2003). Corresponding kinetic parameters are given in Table 2. Here, ν is char formation mass ratio with values 0.35, 0.60, and 0.75 for cellulose, hemicellulose and lignin, respectively (Miller and Bellan 1997).

hemicellulose, and lignin constitute a larger mass fraction of leaf species, they also contain appreciable amounts of lipid and protein (Matt et al. 2020). Note that these latter species are not included in the pyrolysis model here since the kinetic parameters of these two species are not yet known for modeling purposes. Thermophysical properties of the dry fuel constituents, char, and moisture are given in Table 1. The leaf thermophysical properties are calculated using weighted average formulas based on the leaf instantaneous composition and the values in Table 1.

The leaf is subject to convective heating through hot gases exiting the FFB situated at the bottom surface of the computational domain. The FFB exit opening size is 0.18×0.25 m ($x \times y$). Hot gases with 10 mol% oxygen enter the domain at 1000°C and at a velocity of 0.6 m/s as in previous experiments (Prince 2014; Prince and Fletcher 2014; Borujerdi and Shotorban (2022). The lateral surfaces of the domain are modeled as solid walls with no slip condition and fixed ambient temperature. The top surface is modeled as an open boundary.

To model the pyrolysis of the dry fuel, a kinetic scheme with ten reactions proposed by Miller and Bellan (1997) for a dry biomass consisting of cellulose, hemicellulose, and lignin was utilized. The validation of the pyrolysis model implemented here was previously conducted by Miller and Bellan (1997) and Shotorban et al. (2018) against TGA data of Koufopanos et al. (1989). Moisture evaporation is also described by a first-order Arrhenius reaction (Bryden et al. 2002). The reaction scheme is shown in Figure 2 and the kinetic parameters for this scheme are given in Table 2. Char oxidation is not accounted for in this work. Char oxidation may take place upstream of the flame where there is sufficient oxygen. However, Burrows (2001) who experimentally investigated the burning of different kinds of wildland fuels observed that for leaves, the contribution of the flaming combustion to the leaf mass loss is much larger than the contribution of the char oxidation.

Table 2. Reaction kinetic parameters for moist solid fuel thermal degradation (Shotorban et al. 2018) with pyrolysis reactions $R_1 - R_4$ for cellulose (C), hemicellulose (H) and lignin (L) (Miller and Bellan 1997), and moisture evaporation R_5 (Bryden and Hagge 2003).

Reaction	$A(1/s)$	$E(kJ/mol)$	$\Delta h(kJ/kg)$
R_1 (C)	2.80×10^{19}	242.4	0
R_2 (C)	3.28×10^{14}	196.5	225
R_3 (C)	1.30×10^{10}	150.5	-20
R_1 (H)	2.10×10^{16}	186.7	0
R_2 (H)	8.75×10^{15}	202.4	225
R_3 (H)	2.60×10^{11}	145.7	-20
R_1 (L)	9.60×10^{8}	107.6	0
R_2 (L)	1.50×10^{9}	143.8	225
R_3 (L)	7.70×10^{6}	111.4	-20
R_4	4.28×10^{6}	108	-42
R_5	5.13×10^{10}	88	2260

3. Composition-reaction models

3.1. Light gas combustion model

The average composition of the light gas from pyrolysis of the plant species measured by Safdari et al. (2018) is tabulated in Table 3. It is noted that the composition given in Table 3 is on a dry mass basis. Thus, considering live species and referring to Figure 2, gases produced by reaction R_3 consists of $\sim$ 60% (on mass basis) CO, 29% CO_2, 9% CH_4, and 2% H_2. Based on this light gas composition (which is the most inclusive one), other simpler compositions are derived. Table 4 shows different light gas compositions studied in the current work. It can be seen that compositions a and b are the simplest compositions in terms of the number of species involved. They represent the released light gas by only CH_4 and only CO, respectively. As reviewed in § 1, this approach has been used frequently. In composition c, which includes both CH_4 and CO, weight percent of CO is assumed to be the actual value reported in the experiments (Safdari et al. 2018) and then rest is assumed to be CH_4. Composition d deviates from the experimentally measured composition (composition e) with H_2 excluded. This difference allows us to investigate the impact of H_2. In accordance

Table 3. Average composition of light gas from pyrolysis of dead and live plant species (Safdari et al. 2018).

Gaseous Species	Dead Plant	Live Plant
CO	58.5	59.8
CO_2	30.2	29.3
CH_4	9.8	9.0
H_2	1.5	1.9

Table 4. Considered light gas compositions with their respective heat of combustion.

Composition	a	b	c	d	e
CO wt%	–	100	60	60	60
CO_2 wt%	–	–	–	30	29
CH_4 wt%	100	–	40	10	9
H_2 wt%	–	–	–	–	2
$\Delta \bar{h}_c$ (MJ/kg)	50	10.1	26.1	11.1	13

Table 5. Chemical reactions used in the composition-reaction models. Kinetic parameters for reactions 2 and 3 are taken from McGrattan et al. (2013), for reaction 4 from Turns (1996), and for reaction 5 from Miller and Bellan (1997). Here, Z, E, and β are pre-exponential factor, activation energy, and temperature exponent, respectively.

No.	Reaction	Z	E (J/mol)	β	Δh_c (MJ/kg)
1	$CH_4 + 2O_2$ -> $CO_2 + 2H_2O$	N/A	N/A	N/A	50
2	$CO + 0.5O_2$ -> CO_2	1.5×10^9	4.184×10^4	0	10.1
3	CO_2 -> $CO + 0.5O_2$	6.16×10^{13}	32.8×10^4	-0.97	-6.4
4	$H_2 + 0.5O_2$ -> $2H_2O$	6.0×10^{10}	16.4×10^4	0	120
5	Tar -> Light Gases (Refer to § 3.2)	3.0×10^6	10.8×10^4	0	0.042

with the compositions in Table 4, chemical reactions for CH_4, CO, CO_2, and H_2 in Table 5 are considered. Since the combustion of CH_4 assumed to be mixing-controlled and infinitely fast, its kinetic parameters are not displayed. It is noted that the capability of FDS on the DNS mode, where a combination of finite rate and infinitely fast reactions was used, was previously demonstrated by comparing FDS results against the experimental data for a Smyth burner configuration (McGrattan et al. 2013).

3.2. Tar breakdown model

Tar participates in both R_2 (tar formation) and R_4 (tar destruction) in Figure 2. Tar cracking process in which tar is decomposed into light gas, is a secondary pyrolysis process which may occur as a result of tar heat up in the flame zone, and can influence species distribution in the flame (Wurzenberger et al. 2002). The kinetic parameters for the tar breakdown is shown in Table 5. To model the tar breakdown, the following generic one-step reaction scheme is proposed:

$$C_aH_bO_c \rightarrow \nu_{CH_4}CH_4 + \nu_{CO_2}CO_2 + \nu_{CO}CO + \nu_{H_2}H_2 + \nu_C C, \tag{1}$$

where the reactant is assumed a single tar molecule and the product is assumed to consist of the light pyrolysis gases considered in the previous subsection and soot (C).

Considering the relative number of atoms of the reactant and the number of molecules in the product in the chemical reaction above, the following system of under-determined equations governs ν's

$$\mathbf{A}\mathbf{x} = \mathbf{b}, \tag{2}$$

where $\mathbf{x} = [\nu_{CH_4}\, \nu_{CO_2}\, \nu_{CO}\, \nu_{H_2}\, \nu_C]^T$, and $\mathbf{b} = [a\ b\ c]^T$. Additionally, the constraint

$$\mathbf{x} \geq \mathbf{0}, \tag{3}$$

must be satisfied for the non-negativity of the stoichiometric numbers of the products in Eq (1).

Balancing the reaction in Eq (1) results in

$$\mathbf{A} = \begin{bmatrix} 1 & 1 & 1 & 0 & 1 \\ 4 & 0 & 0 & 2 & 0 \\ 0 & 2 & 1 & 0 & 0 \end{bmatrix}. \tag{4}$$

In Eq (1), $\mathbf{b}$ is set to

$$\mathbf{b} = \begin{bmatrix} 11.53 & 9.13 & 0.64 \end{bmatrix}^{\mathrm{T}}, \tag{5}$$

to be consistent with the a, b and c values, viz. $C_{11.53}H_{9.13}O_{0.64}$, provided by Thomas H. Fletcher of Brigham Young University based on the averaging of tar composition across 15 live plant species measured by his research group in the study of the pyrolysis gases released from plants under heating (Safdari et al. 2018; Safdari 2018). He also provided the average nitrogen atoms of 0.03 for the tar molecule, which is neglected here because it is much smaller than the other atom numbers.

It can be readily shown that matrix **A** in Eq (4) has full rank; hence, Eq (2) has infinitely many solutions for **x** (Datta 2010). To find the general solution, since **A** is a 3×5 matrix, three of the unknowns, e.g., the first three elements of **x**, are selected to be expressed in terms of the remaining two unknowns using Eqs (2), (4) and (5)

$$\nu_{\mathrm{CH_4}} = -0.5\nu_{\mathrm{H_2}} + 2.2825, \tag{6}$$

$$\nu_{\mathrm{CO_2}} = -0.5\nu_{\mathrm{H_2}} + \nu_{\mathrm{C}} - 8.6075, \tag{7}$$

$$\nu_{\mathrm{CO}} = \nu_{\mathrm{H_2}} - 2\nu_{\mathrm{C}} + 17.8550, \tag{8}$$

and then the non-negativity conditions in Eq (3) are applied on all unknowns

$$0 \leq \nu_{\mathrm{H_2}} \leq 4.5650, \tag{9}$$

$$0.5\nu_{\mathrm{H_2}} + 8.6075 \leq \nu_{\mathrm{C}} \leq 0.5\nu_{\mathrm{H_2}} + 8.9275. \tag{10}$$

Using Eqs (6-10), a solution can be obtained by the following algorithm: (a) Choose a value for $\nu_{\mathrm{H_2}}$ from the range specified in Eq (9); (b) Choose a value for ν_{C} from the range given in Eq (10); (c) Calculate $\nu_{\mathrm{CH_4}}$, $\nu_{\mathrm{CO_2}}$ and ν_{CO} using Eqs (6-8), respectively. It is evident that $\nu_{\mathrm{C}} = 0$ does not satisfy the conditions in Eqs (9) and (10). This means that the assumption of carbon production is a necessary condition for the existence of a solution to Eqs (2-5). However, a vanishing stoichiometric number is possible for the rest of the product molecules in the model reaction above.

For an underdetermined system of equations, such as Eq (2), there is often an interest in the solution that minimizes **x** via the linear least-square criterion, viz.

$$\arg\min_{\mathbf{x}} \| \mathbf{x} \|_2^2, \tag{11}$$

where $\| \mathbf{x} \|_2$ indicates the magnitude of **x**. This is $\mathbf{x} = \mathbf{A}^{\mathrm{T}}\left(\mathbf{A}\mathbf{A}^{\mathrm{T}}\right)^{-1}\mathbf{b}$, aka the minimum-norm solution (Datta 2010), for a general underdetermined system Eq (2) if **A** has full rank. However, the solution obtained through this approach for **A** and **b** specified in Eqs (4) and (5) does not satisfy the non-negativity constraint in Eq (3). To satisfy this, the optimization problem in Eq (11) is solved with an objective function where in addition to $\| \mathbf{x} \|_2^2$, the equality and inequality constraints in Eq (2) and Eq (3) are included with their associated Lagrangian multipliers. Although this solution can be analytically obtained, the MATLAB function lsqlin is used here to find it numerically because of its faciliness

$$\mathbf{x} = \begin{bmatrix} 2.2825 & 0.0000 & 0.6400 & 0.0000 & 8.6075 \end{bmatrix}^{\mathrm{T}}. \tag{12}$$

It can be readily shown that the solution above is identical to a solution obtained via Eqs 6-10) where ν_{H_2} and ν_C are set to the lower bounds of inequalities in Eqs (9) and (10), viz. $\nu_{H_2} = 0$ and $\nu_C = 8.6075$. Since $\nu_{H_2} = \nu_{CO_2} = 0$ in Eq (12), this corresponds to assuming only CH_4, CO and C are produced in the tar breakdown reaction Eq (1). Although the solution in Eq (12) minimizes the stoichiometric numbers, the significance of this minimization from the chemistry standpoint is not known.

Among solutions to Eqs (6-10), there are others which might be also of interest. For example, setting $\nu_{H_2} = 0$ and $\nu_C = 8.9275$, corresponding to the lower bound of Eq (9) and upper bound of Eq (10) results in

$$\mathbf{x} = \begin{bmatrix} 2.2825 & 0.3200 & 0.0000 & 0.0000 & 8.9275 \end{bmatrix}^T, \tag{13}$$

which corresponds to the assumption that only CH_4, CO_2 and C are produced. Similarly, other solutions using the upper bound of ν_{H_2} and the lower or upper bounds of ν_C may be obtained. Setting $\nu_{H_2} = 2.2825$ and $\nu_C = 9.9087$, the midpoints in the ranges given in Eqs (9) and (10), respectively, results in

$$\mathbf{x} = \begin{bmatrix} 1.1413 & 0.1600 & 0.3200 & 2.2825 & 9.9087 \end{bmatrix}^T. \tag{14}$$

3.3. Modeling scenarios

In this work, seven models based on a combination of different light gas compositions and chemical reactions are used to represent the gas-phase chemical kinetics. Each composition-reaction model is identified by a combination of a letter and numbers. The letter denotes the light gas composition according to Table 4 and the numbers denote the reactions describing chemical evolution of the corresponding composition according to Table 5. For example, Model a1 assumes all the pyrolysis gas is CH_4 which undergoes reaction 1 in Table 5. Model e1–4 assumes the pyrolysis gas composition is 9% CH_4, 60% CO, 29% CO_2, and 2% H_2 and the chemical conversion of this mixture is governed by reactions 1 to 4 in Table 5. Among the seven models, two models (a1 and b2) are single-species single-reaction models and the rest (c1&2, d1–3, e1–4, d1-3&5, and e1–5) are multi-species multi-reaction models. In all scenarios, tar formation and decomposition reactions (R2 and R4, respectively, in Figure 2) occur in the leaf. Note that not all the tar produced by reaction R2 is consumed by reaction R4. The remaining tar is transported from the leaf into the surrounding. In models a1, b2, c1&2, d1–3, and e1–4, tar in the surrounding gas remains inert while in models d1-3&5 and e1–5 tar reacts in the gas domain according to tar breakdown model discussed in Section 3.2. Models d1-3&5 and e1–5 are extensions to Models d1–3 and e1–4, respectively, through inclusion of tar breakdown (reaction 5 in Table 5) so that the impact of tar breakdown can be investigated.

4. Results and discussions

Figure 3 displays the temporal evolution of the normalized mass of manzanita leaf based on averaged experimental data reported in Prince (2014) and results from current simulations using composition-reaction models explained as undefined. During the experiments, mass of the leaf was recorded by a cantilever mass balance, which was synchronized and time-

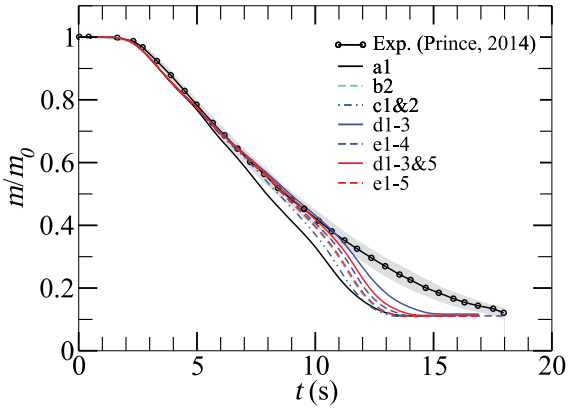

Figure 3. Time evolution of the leaf mass normalized by the leaf initial mass in the experiments (averaged of 18 runs) (Prince 2014) and current simulations with different composition-reaction models. In the model names, the letter denotes the pyrolysis gas composition and the numbers indicate the reactions used to describe chemical evolution of the pyrolysis gas. Shaded area is 95% confidence interval for the experimental data.

stamped with video images (Prince 2014). It can be seen that the leaf mass loss is virtually insensitive to the composition-reaction model up to ~ 4.5 s. This behavior can be attributed to the fact that up to this time, mass loss is dominated by moisture evaporation to be discussed later. Since the simulated leaf has the same FMC in all cases, their corresponding predicted normalized masses are the same. After this time, the mass loss in Model a1, where the pyrolysis gas is represented only by CH_4, progresses faster and thus, exhibits the largest deviation from the corresponding experimental data. This is because CH_4 has a relatively large heat of combustion (~ 50,000 kJ/kg) which results in a relatively large heat release rate and therefore, the leaf receives more heat flux which accelerates its decomposition process. Models c1&2 in which the pyrolysis gas is assumed to be 40 wt% CH_4 and 60 wt% CO, shows the second largest deviation from the experimental data but this deviation is appreciably smaller compared to the deviation exhibited by Model a1. The reason is that the overall heat of combustion of the pyrolysis gas $\Delta\bar{h}_c$, in this model, is smaller because of the relatively small heat of combustion of CO (~ 10,100 kJ/kg). When no CH_4 is included in the pyrolysis gas and it is represented only by CO, as in Model b2, a slight improvement in the mass prediction compared to Model c1&2 is observed.

In Figure 3, Models d1–3 and d1-3&5 exhibit the best match with the experimental data as far as the difference between experimental and modeling mass versus time is concerned. This is further evident in Figure 4 where the relative difference between the numerical and experimental mass is plotted versus time. In both these models, the pyrolysis gas comprises of 10 wt% CH_4, 60 wt% CO, and 30 wt% CO_2. The only difference between these models is that the tar breakdown reaction. We examined both Eqs (12) and (14) for the tar breakdown model in this work. However, the leaf mass loss behavior did not exhibit a remarkable sensitivity to which equation was used. The results shown for the composition-reaction models with the tar breakdown reaction, i.e., d1-3&5 and e1–5, are based on Eq (12). In both d1–3 and d1-3&5 models, only a fraction of the pyrolysis gas (CH_4 and CO) is combustible whereas in Models a1, b2, and c1&2 the entire pyrolysis gas

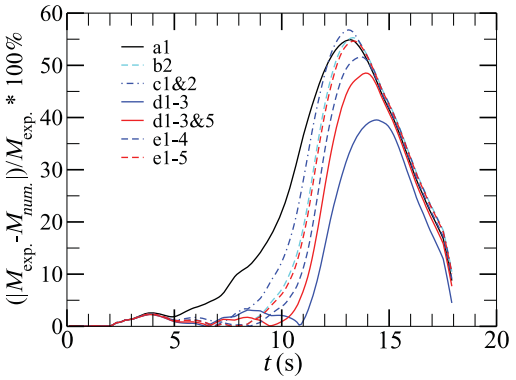

Figure 4. Time history of the relative difference between numerical and previous experimental normalized mass Prince (2014) for various composition-reaction models investigated.

is combustible. Furthermore, the associated reaction with CO_2 (Reaction 3 in Table 5) is endothermic, meaning that it absorbs heat to proceed. For these two reasons, less heat transfers to the leaf when Models d1–3 and d1-3&5 are implemented. Hence, leaf pyrolysis progresses more slowly, and consequently these models agree better with the experimental data in terms of the mass evolution. This finding is consistent with that of Tihay et al. (2009) who studied combustion of pyrolysis gas released from crushed Mediterranean forest fuels. In Tihay et al. (2009), when the gas phase chemical kinetics was modeled by a mixture of CH_4, CO, and CO_2 and their associated reactions, a reasonable match with the experimental data for flame temperature was achieved. Comparing Models d1–3 and d1-3&5 in Figure 3 suggests that the inclusion of tar cracking in the model somewhat accelerates the mass loss after $t = 11$ s. This acceleration is likely because at least a portion of the overall heat released by the combustion of secondary pyrolysis products provides additional heat feedback to the leaf.

When in Models e1–4 and e1–5, pyrolysis gas composition is matched with the experimentally measured one, the solid fuel mass loss slightly accelerates compared to Models d1–3 and d1-3&5. This is because in Models e1–4 and e1–5 the light gas composition is 9 wt% CH_4, 60 wt% CO, 29 wt% CO_2, and 2 wt% H_2. Although H_2 yield is small, because its heat of combustion is very large ($\sim$ 121,000 kJ/kg), the presence of H_2 exhibits an impact on the overall heat release rate and thus, the solid fuel decomposition. Again, it is noted that the inclusion of tar cracking in Model e1–5 accelerates the leaf mass loss.

Another important factor that could contribute to the distinct mass loss behaviors observed in Figure 3, is different oxygen consumption behaviors for different fuel species. It is noted that the O_2 consumption behavior for a specific fuel species is implicitly accounted for through the kinetics parameters (such as O_2 reaction order) used to describe the reaction rate of that fuel species.

Shown in Figure 5 are the simulated time histories of the solid fuel mass loss rate (MLR) and heat release rate (HRR) in the gas phase. It is noted that experimental data for these quantities are not given by Prince (2014). In Figure 5(a), it can be seen that for all models, MLR initially remains zero from $t = 0$ to $\sim$ 1 s. Over this time period, the leaf undergoes

heating without losing mass. Subsequently, a rapid rise is noted for MLR, it then attains a peak value, and then slightly decreases. The time period from $t = 1$ to ~ 4.5 s is when moisture evaporation dominates the mass loss process. That is why MLR curves in Figure 5(a) are nearly the same in this time period, given that the FMC is the same for all models. Differences in the MLR curves start to appear shortly after the pyrolysis process starts to dominate the leaf mass loss.

It is observed that for most of the time period between $t = 4.5$ and ~ 9 s, MLR for Model a1 with methane as the only pyrolysis gas, exhibits the largest values. This behavior is mainly attributed to the fact that in this time interval, the heat release rate in Model a1 is the largest, as could be seen in Figure 5(b). As a result, the solid fuel receives a larger heat flux, its temperature rises more rapidly, and consequently it loses mass at higher rates.

Model d1–3 displays the smallest overall value for MLR in the interval between $t = 4.5$ and ~ 12 s. Note that in Model d1–3 the light gas has a composition of 10 wt% CH_4, 60 wt % CO, and 30 wt% CO_2. As shown in Figure 5(b), this model results in the least amount

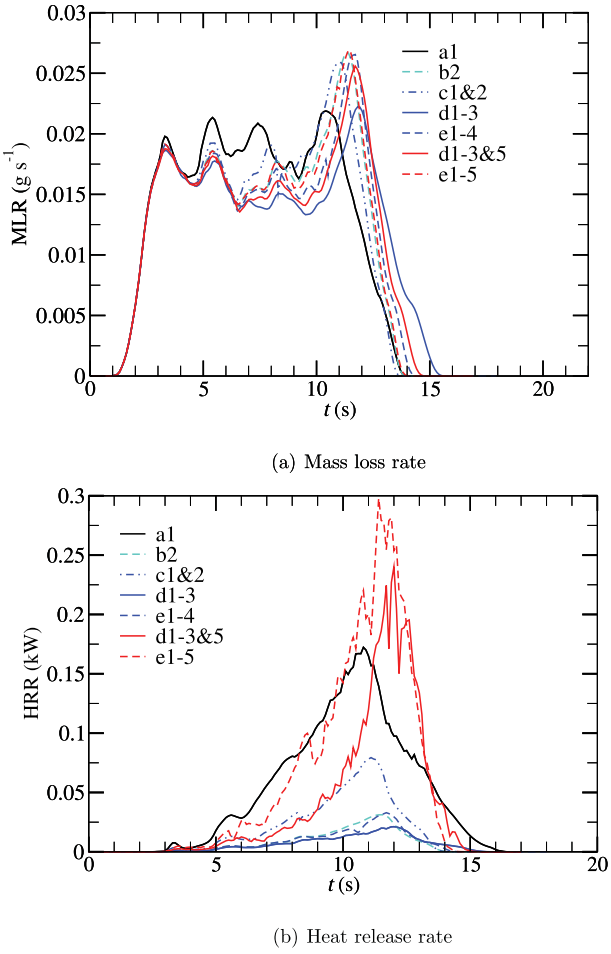

Figure 5. Time evolution of (a) the leaf mass loss rate, and (b) heat release rate in the gas phase for simulations with different composition-reaction models.

of heat release rate due to the fact that it has the least heat of combustion among all models. Thus, the leaf pyrolysis rate is the slowest for most of the time. Consequently, when Model d1–3 is applied, the leaf thermal decomposition takes the longest time of ~ 15.5 s.

It is evident from Figure 5(b) that all HRR curves start to gain appreciable amounts at around $t = 3$ s. This initial similarity, as illustrated in Figure 5(a), is correlated with the initial similarity in the pyrolysis rates (or MLRs) between all cases. Despite the differences in the composition-reaction models, the onset of pyrolysis in the leaf in all scenarios is similar and initial release of appreciable amount of pyrolysis is noted to occur around $t = 3$ s. After $t = 3$ s, Model a1 displays the largest HRR values because of the largest heat of combustion of the pyrolysis gas for this model as discussed earlier. If the time at which HRR reaches its first local peak is assumed to represent the ignition time, then for all cases ignition time is ~ 3.3 s. It is noted that ignition times were not reported in Prince (2014) for comparison. However, in similar burning experiments on manzanita leaves with FMC 65%, an ignition time of 3.1 s was reported by Borujerdi and Shotorban (2022). It is noted that in the burning experiments Borujerdi and Shotorban (2022), ignition time is the time at which the first sustainable flame was observed. However, in the simulations here, the ignition time is determined based on when the HRR first exhibits a local peak. This difference in ignition criterion could be a reason for the difference between the experimental and predicted ignition times.

The HRR curves exhibit a similar trend in Figure 5(b). They start to rise around 3 s, later reaching a maximum value, and eventually dropping to zero. The times of attainment of the maximum and zero HRR are consistent with the corresponding times in the MLR curves depicted in Figure 5(a). This consistency is because MLR and HRR are strongly related to each other. In the other words, when MLR increases, gaseous fuel is generated from the leaf pyrolysis and released into the surrounding gas at a higher rate and results in larger HRR due to the fuel combustion. By the same token, when MLR decreases and approaches zero, HRR drops and approaches zero as well. The computed HRR for Models d1-3&5 and e1–5, which account for the tar breakdown, exceed the computed HRR of Model a1 within specific time intervals. For example, HRR of Model d1-3&5 becomes larger than that of Model a1 from $t = 11$ to $t = 13.5$ s. At the first glance this seems to contradict with the fact that the overall heats of combustion of the pyrolysis gases, $\Delta\bar{h}_c = \sum_{j=1}^{N} y_j \Delta h_{c,j}$, corresponding to Models d1-3&5 and e1–5 are smaller than the heat of combustion of the pyrolysis gas of Model a1. However, according to the tar breakdown reaction, tar decomposes into CH_4, CO, and C, resulting in additional gaseous fuel species, which undergo combustion reactions and increase the overall heat release rate.

Figure 6(a) displays the time histories of the leaf average surface temperature for different composition-reaction models. It is noted that for almost the first 5 s, the temperature is not sensitive to the composition-reaction models, which is due to the fact that water evaporation is the dominant phenomenon initially and is handled similarly in all models. After this initial time period, the temperature starts to rise with different rates for the composition-reaction models. Models a1 and d1–3 exhibit the fastest and slowest temperature rise, respectively. This is because the surface temperature and the mass evolution are interlinked. A faster mass loss indicates a larger mass loss rate. As previously demonstrated, a larger mass loss rate results in a larger heat release rate in the surrounding gas. Consequently,

more heat is available to be transferred back into the solid fuel by means of convection and radiation, which increases solid fuel temperature. It can be seen that all the simulated average surface temperatures reach the steady state and plateau in the final few seconds. This is because in all the simulations, the solid fuel burnout (a state at which the solid fuel has been completely pyrolyzed and its mass loss terminates) occurs a few seconds before the end of simulations. Since after burnout, the leaf no longer undergoes any thermochemical process, its temperature is stabilized. Figure 6(b) shows the leaf median surface temperature for Model d1–3 and experiments (Prince 2014). In the experiments, surface temperature of one side of the leaf was recorded using a FLIR camera (Thermovision A20, wavelength 7.5–13 μm). At these wavelengths, the IR camera sees the leaf surface but not the soot formed due to the flaming combustion (Prince 2014). The error bars represent 25 and 75 percentiles. Here, from all models, only for model d1–3 the median temperature is shown since its mass loss exhibited the best agreement with the experimentally measured mass loss. A temperature plateau of nearly $\sim T = 465$ K is visible in the experimental data from $t =$ 2 to 5 s. Prince (2014) attributes this plateau to the vaporization of the leaf moisture based on the argument that evaporation is endothermic and tends to stabilize the temperature around the water boiling point (473 K). This plateau is also observed in the simulations at a lower temperature. After the plateau, temperature rises with larger rate for Model d1–3. While in the final few seconds, the modeled median temperature plateaus, the experimental one is still rising. In the experiments, as shown in Figure 3, the pyrolysis is slower than that in the simulation. Therefore, at $t = 18$ s (the last time instance for which the experimental data were given by Prince (2014)) the leaf still pyrolyzes and thus, its temperature changes and does not exhibit a plateau.

The average surface temperature of the leaf is plotted against the fractional leaf conversion defined as $\alpha = 1 - m/m_0$ in Figure 6(c). The temperature plateau can also be observed in this figure. In the experiments, the plateau extends from $\alpha = 0.05$ to $\alpha = 0.25$ which corresponds to $t = 5$ s, consistent with the results presented in Figure 6(a). In the simulations, the plateau extends within the same range but at a lower temperature. Since α is simply related to the leaf mass, and the latter is correlated with the leaf temperature, the same behavior is noted here as in Figure 6(a), regarding how the simulated T vs α for different composition-reaction models is compared with the experimental T vs α behavior.

The discrepancies between the modeling results and their corresponding experimental data could be attributed to several factors. Chief among them are the solid fuel pyrolysis kinetic model, the assumed rectangular shape for the leaf, and the composition-reaction model. All reactions that are used here and given in Table 5 are global reactions. Global reactions may overestimate the flame temperature (Zhou and Pereira 1998) compared to when a skeletal or full reaction mechanism is used. This overprediction can result in overestimation of the heat feedback to the leaf, and consequently in overestimation of the leaf temperature. Furthermore, the composition of the pyrolysis gas (Safdari et al. 2018) used here was measured under experimental conditions, which are not fully consistent with the ones in the simulations here or the experiments of Prince (2014). The experiments of Safdari et al. (2018) were carried out in an environment free of any oxidizing agent to prevent flaming combustion. Moreover, in those experiments, the temperature of the gas stream used as the heating source was reported to be $\sim 765^\circ$ C near the leaf, which is lower than $\sim 1000^\circ$ C reported in the experiments for the heat source temperature near the leaf (Prince 2014; Gallacher 2016) and simulations here. It is noted that formation of the flame

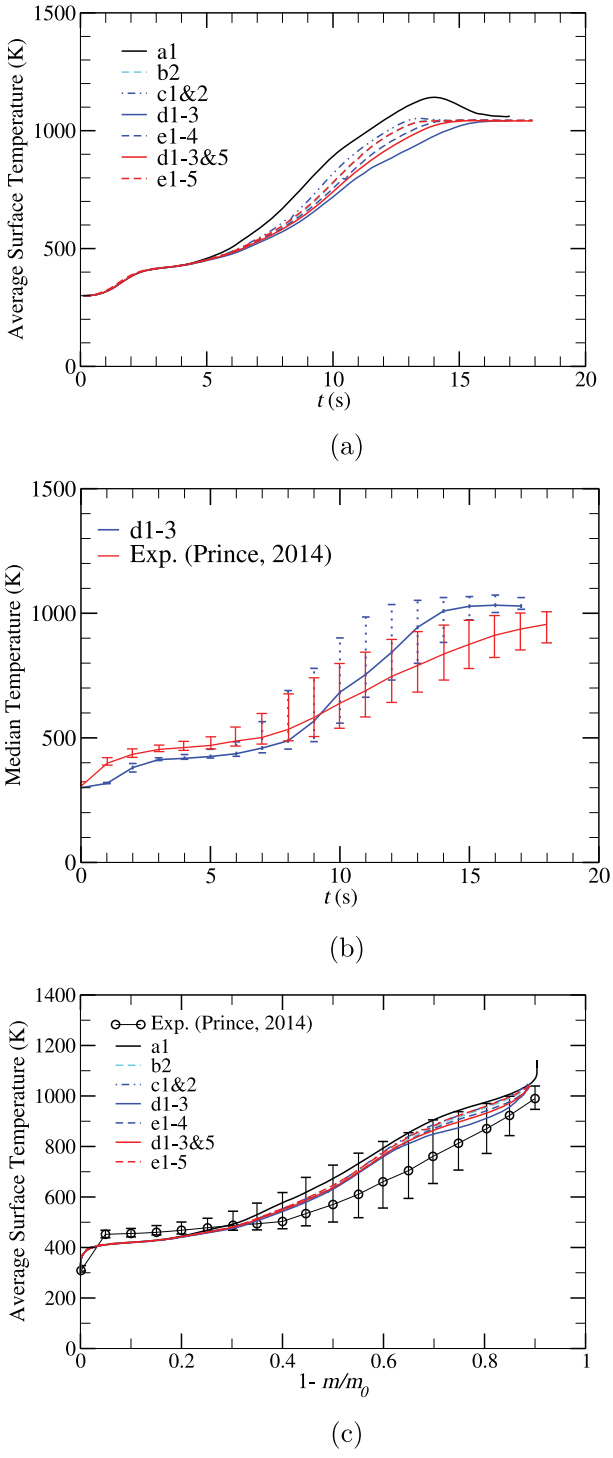

Figure 6. (a) temporal variation of the average surface temperature of the leaf; (b) temporal variation of the median surface temperature of the leaf; and (c) the average surface temperature of the leaf versus leaf conversion. The error bars represent the $25^{th}/75^{th}$ percentiles.

in the experiments of Prince and simulations here further increases the temperature. The yield of different gaseous species in the pyrolysis products is dependent on temperature. For Models d1-3&5 and e1–5 which include tar breakdown, additional source of discrepancy could be how tar breakdown is modeled. It should be noted that lumping the very complicated heavy tar into a single species as $C_{11.53}H_{9.13}O_{0.64}$ and assuming its breakdown to take place through a single-step global reaction are simplifications made in the current work. In fact, tar is a complex mixture of condensable hydrocarbon compounds consisting of oxygenated hydrocarbons and polycyclic aromatic hydrocarbons (Ni et al. 2006). The yields of different tar constituents not only depend on the plant species but also on the heating conditions (Safdari et al. 2020). Hence, the chemistry governing the decomposition of tar during the secondary pyrolysis can be very involved compared to the decomposition reaction mechanism adopted in this manuscript.

Figure 7 shows the gas-phase temperature contours on $x = 0$ m plane, at $t = 10$ s for three Models a1, c1&2, and b2 corresponding to the CH_4 yield of 100, 40 and 0 wt%, respectively. Here, a time of $t = 10$ s is chosen since it is when the flame is growing and the leaf MLR is rising and approaching its maximum. According to Figure 5(b), HRR for Model a1 is 143 W at $t = 10$ s is the largest among all models. This indicates that more energy per unit time is released from combustion reaction(s). As a result, the gas-phase temperature reaches higher values around the reaction zone. Moreover, by means of convective transport of heat in the gas, further downstream locations in the gas domain are heated by the flame. Hence, the thermal plume is expected to be longer as can be observed in Figure 7(a). Figure 5(b) shows that at time 10 s, the HRR of Model c1&2 is 55 W, which is smaller than that in Model a1 by approximately a third. This difference is correlated with the fact that the temperature rise near the flame zone is less appreciable and thermal plume is smaller in Model c1&2 compared to Model a1, as may be observed in Fig. 7(a,b). In Figure 7(c), which corresponds to Model b2 with no methane yield in the pyrolysis gas, the temperature rise is due to combustion of CO and is minimal compared to the other models which include methane. An indication of this limited rise is small yellow spots near the trailing edge of the leaf. According to Figure 5(b), HRR for this model at $t = 10$ s is 19 W, which is a substantially smaller value compared to the other two models. This difference is due to relatively small heat of combustion of CO in Model b2. It could be said that, due to CH_4 relatively large heat of combustion, the methane yield in the pyrolysis gas plays a significant role in the temperature rise of the gas phase and consequently the size of the thermal plume.

Shown in Figure 8 are the iso-surfaces of the heat release rate per unit volume (HRRPUV) of 8000kW/m^3 in the gas phase, at $t = 10$ s for Models d1–3 and e1–4 with a difference that Model d1–3 does not include H_2. HRRPUV is calculated by adding up the volumetric heat release rates for all reactions in the model. Comparing Figure 8(a,b) reveals that H_2, even with very low yield as in here, influences HRRPUV. This is attributed to the very large heat of combustion of H_2 which is $\sim$ 121,000 kJ/kg. This observation is also consistent with the observation in Figure 5 where an overall larger HRR was noted for model e1–4. The size of the iso-surface in Figure 8(b) is greater, suggesting that a larger portion of the gas domain is heated up by the energy release from combustion. As a result, the overall thermal energy transferred to the leaf for model e1–4 is larger compared to that for model d1–3. As a result, the heat flux from the flame to the solid fuel is greater in Model e1–4 and consequently, the leaf temperature rises more rapidly in this model. This difference is consistent with Figure 6(a), where at $t = 10$ s the average surface temperatures in

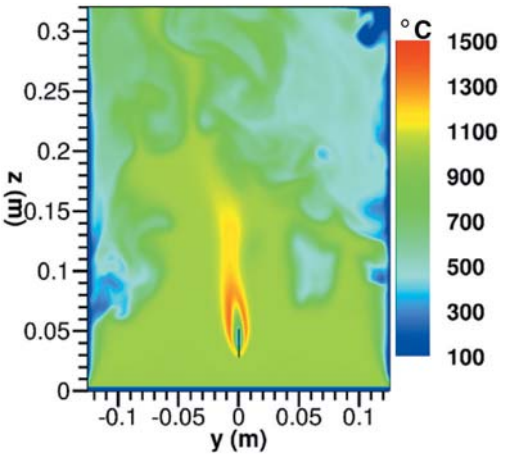

(a) Model a1

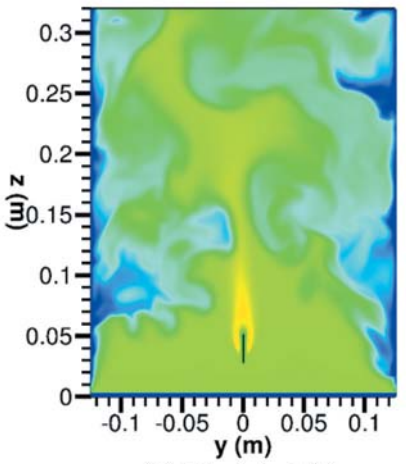

(b) Model c1&2

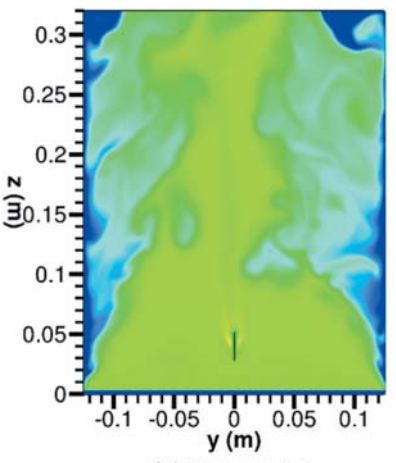

(c) Model b2

Figure 7. Contour plots of the gas phase temperature on $x = 0$ plane, at $t = 10$ s, and for (a) model a1 with CH_4 yield of 100 wt%, (b) model c1&2 with CH_4 yield of 40 wt%, and (c) model b2 with CH_4 yield of 0 wt%.

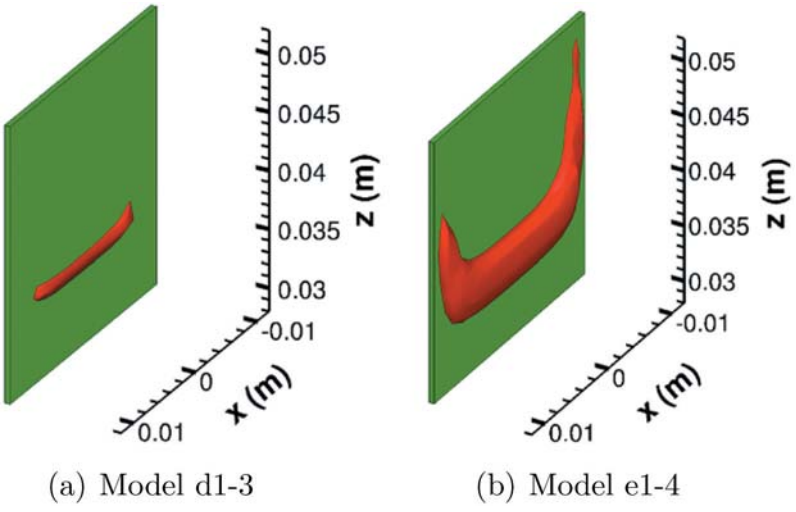

Figure 8. Iso-surfaces of heat release rate per unit volume of 8000kW/m^3 at $t = 10$ s for (a) model d1–3 with H_2 yield of 0 wt%, and (b) model e1–4 with H_2 yield of 2 wt%.

Model e1–4 is greater than Model d1–3. Accordingly, in Figure 5, Model e1–4 displays a value larger than Model d1–3 for MLR at this time.

Figure 9 displays contours of the mass fractions of tar and CO, and heat release rate per unit volume on the $x = 0$ m plane at $t = 12.5$ s for Models d1–3 and d1-3&5. In both models, the pyrolysis gas composition is 10 wt% CH_4, 60 wt% CO, and 30 wt% CO_2. The difference between these two models is that the tar breakdown is accounted for in Model d1-3&5 through Reaction 5 from Table 5. It is noted that $t = 12.5$ s is nearly the time when both MLR and HRR reach their peak. It is seen in Figure 9(a,b) that a substantial amount of tar remains in the vicinity of the leaf in both models. Large mass fractions of tar seen here is consistent with the experimental findings of Safdari et al. (2018); Amini et al. (2019); Safdari et al. (2020), who reported large tar yields in the investigated plant species. However, downstream of the leaf, for $z > 0.08$ m, tar mass fraction in Model d1-3&5 is much smaller than in Model d1–3. The reason for this difference is that in Model d1-3&5, tar breakdown reaction is taken into account and as a result of this reaction, tar is consumed downstream of the leaf whereas it is not in Model d1–3. It is noted that tar decomposition to the primary light gases takes place at high temperatures (generally $T > 500°C$ (Scott et al. 1985)) and sufficiently long residence times (Antal 1983, 1985; Evans and Milne 1987). The need for high temperatures for tar cracking can also be understood from the fact that the pre-exponential factor of the tar breakdown reaction (Miller and Bellan 1997) is relatively small ($O(10^3)$ and $O(10^4)$ smaller than that for CO and H_2 reactions, respectively). The temperature downstream of the leaf, as determined in Figure 7, is considerably larger than 500°C. Moreover, a region right above the leaf trailing (top) edge may be in the wake of the hydrodynamic boundary layers formed on the leaf lateral faces. Therefore, the gas in this region has a smaller velocity and thus, a longer residence time which can facilitate tar cracking. As a result of the tar cracking downstream of the leaf in Model d1-3&5, as seen in Figure 9(b), the mass fraction of CO that is produced from secondary pyrolysis is significant

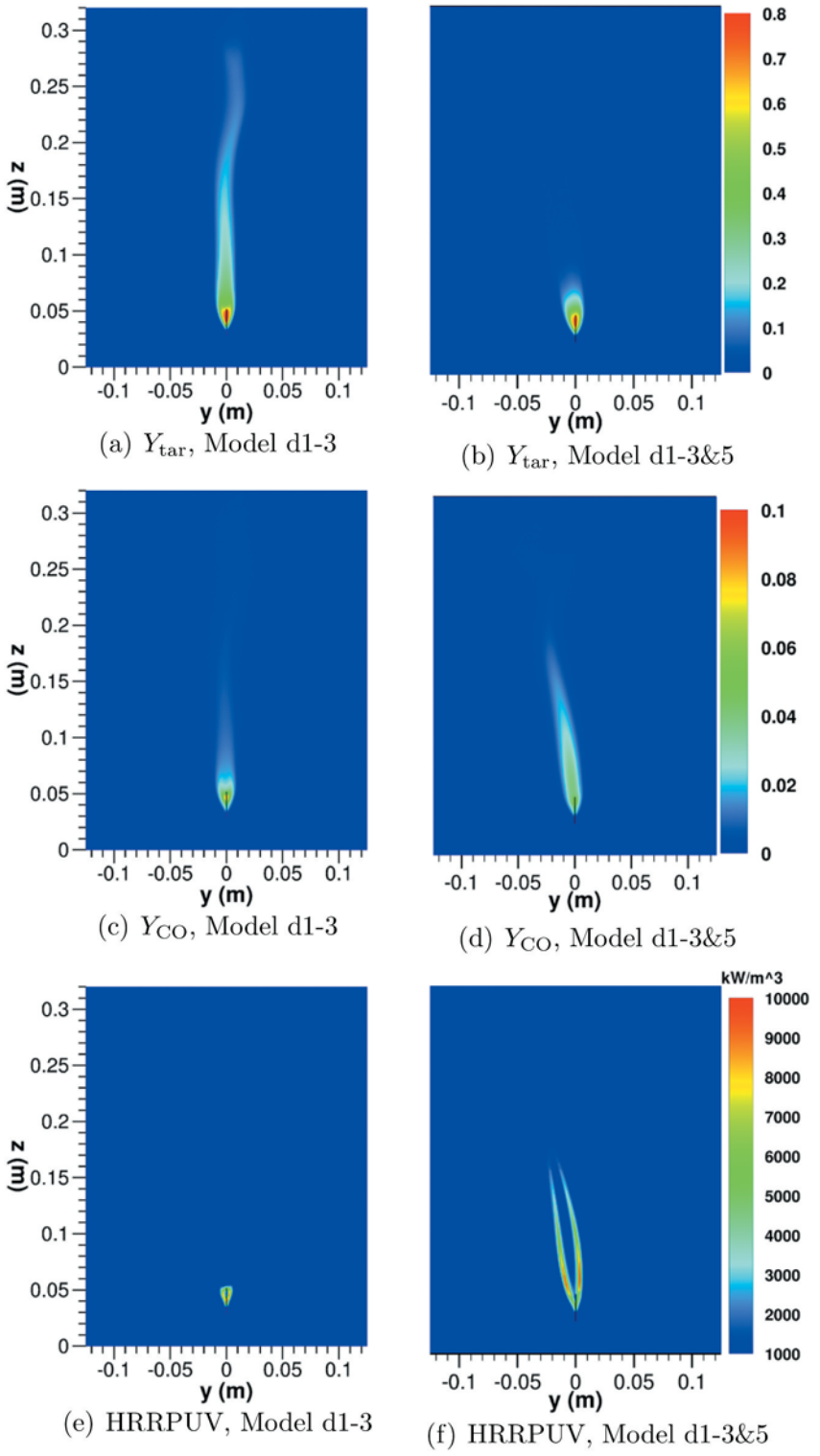

Figure 9. Contours of the mass fractions of (a,b) tar and (c,d) CO, and (e,f) heat release rate per unit volume on $x = 0$ m plane and at $t = 12.5$ s for composition-reaction models d1–3 (left panels) and d1-3&5 (right panels).

therein (Figure 9(d)). In contrast, considerably less CO is noted in Figure 9(c) where the tar breakdown is not accounted for. In this subfigure, all CO is produced by primary pyrolysis.

The products of tar breakdown, as discussed in § 3, are CH_4, CO, and C. Therefore, in the region where the secondary pyrolysis process occurs, gaseous fuel is generated and subsequently undergoes combustion. Hence, not only heat is released in the vicinity of the leaf due to combustion of primary pyrolysis products but also heat is released further away from the leaf due to combustion of secondary pyrolysis products, as could be seen in Figure 9(F). As a result, the heat flux from the gas phase to the solid fuel increases, causing the leaf to gain a higher average temperature and mass loss rate as seen in Figures 6 and 5, respectively. On the other hand, when tar cracking is not accounted for, as in Model d1–3, all of the heat released in the gas phase originates from the combustion of gaseous fuels which are products of the primary pyrolysis. As soon as these light gases are transported into the gas domain, they are exposed to sufficiently large temperatures ($\sim$1000° C) and ignite in the vicinity of the leaf. Accordingly, the reaction zone wherein heat is released will be limited to the close neighborhood of the leaf, as noted in Figure 9(e). The presence of a reaction zone adjacent to the fuel particle for a high temperature convective heating, as seen in Figure 9(e, F), is consistent with the experimental observations reported by McAllister and Finney (2017). They observed that for high convective temperature, the ignition and flaming of volatiles occur adjacent to the fuel particle.

5. Conclusions

Combustion of the gaseous components of the pyrolysis products is one of the key processes responsible for spread of fire in wildland fuels. In this study, the influence of the adapted composition of the gas released by the pyrolysis of a manzanita leaf, and the subsequent reaction mechanism implemented to model the combustion of this gas, was computationally investigated. Furthermore, the effect of the secondary pyrolysis, represented by the tar breakdown in the gas phase, was studied. The computational configuration was designed to resemble an experimental setup in which manzanita leaves were burned (Prince 2014). Overall, a combination of seven composition-reaction models for the gas-phase combustion was considered in this study. Among these models, two models were single-species and single-reaction schemes representing the pyrolysis gases with only one species (either CH_4 or CO). The remaining five models were multi-species and multi-reaction schemes. The composition in the most inclusive model was chosen to be consistent with the major gases determined via pyrolysis measurements conducted on live and dead leaves of dozens of plant species (Safdari et al. 2018). They were CO, CO_2, CH_4, H_2, and tar.

Comparison with the previous experimental data (Prince 2014) for the time history of the normalized leaf mass showed that among all models, the model with the pyrolysis gases represented by only CH_4 resulted in the fastest mass loss, exhibiting the largest deviation from the experimental data. The model representing the pyrolysis gases with 10 wt% CH_4, 60 wt% CO, and 30 wt% CO_2, displayed the slowest mass loss and compared the best with the experimental data. This behavior was mostly attributed to the fact that CH_4 has a large heat of combustion compared to CO. Therefore, when the pyrolysis gas was only CH_4, much more heat was released in the gas phase, which resulted in enhanced heat feedback to the leaf and eventually accelerated its pyrolysis. Due to the increased heat feedback to the leaf in case where the pyrolysis gases represented by only CH_4, the average

surface temperature of the leaf was the highest during the simulation. Average surface temperature predicted by this model showed deviations as high as ~ 200 K from the corresponding experimental data. In contrast, average surface temperature predicted by the model in which the pyrolysis gases were 10 wt% CH_4, 60 wt% CO, and 30 wt% CO_2, showed maximum deviation of ~ 50 K from the experimentally measured surface temperature.

When H_2 yield of 2 wt%, as suggested by the measurements of Safdari et al. (2018), was included in the model, even at this low level, it had a significant impact on the overall heat release rate in combustion and thus, the leaf mass loss rate. Simulations shed a light on how the tar breakdown in the gas phase could influence the leaf burning. It was noted that the tar cracking mostly occurred above the leaf where tar might gain longer residence times. As a consequence of the tar breakdown into the light gases, additional fuel species including CO and CH_4 were generated. This extra fuel underwent combustion and thus, additional heat was released in the gas phase. A portion of this heat was transferred back into the solid fuel and somewhat increased its temperature and accelerated its mass loss process.

Thus the overall conclusion in this manuscript is that the combination of pyrolysis gas composition and reaction mechanism adapted has a strong influence on overall leaf burning behavior. The detailed analysis of results provide direct insight into the specific reasons for observed differences between various models. While there could be a surrogate fuel species (Mell et al. 2009b) which may reproduce the leaf burning behavior, since leaves have a complex structure with a variety of constituents, detailed representation of the pyrolysis process in the leaf is of importance. Using a surrogate fuel species would be more appropriate for a larger-scale fire investigation where pyrolysis process is not as important as in this work.

Acknowledgments

The authors acknowledge Thomas H. Fletcher of BYU for providing the tar molecule formula measured by his research group and suggesting to include soot as a product in the tar breakdown reaction. This work was supported by DOD/EPA/DOE Strategic Environmental Research and Development Program project RC-2640 administered by the USDA Forest Service PSW Research Station through cooperative agreement JV-11272167-025 with UAH. High performance computing resources and technical support provided by the Alabama Supercomputer Authority are appreciated.

Disclosure statement

No potential conflict of interest was reported by the author(s).

Funding

This work was supported by the DOD/EPA/DOE Strategic Environmental Research and Development Program [RC-2640]; USDA Forest Service PSW Research Station [JV-11272167-025].

ORCID

Babak Shotorban http://orcid.org/0000-0001-6838-7297
David R. Weise http://orcid.org/0000-0002-9671-7203

References

Amini, E., M. S. Safdari, J. T. DeYoung, D. R. Weise, and T. H. Fletcher. 2019. Characterization of pyrolysis products from slow pyrolysis of live and dead vegetation native to the southern United States. *Fuel* 235:1475–91. doi:10.1016/j.fuel.2018.08.112.

Antal, M. 1983. Effects of reactor severity on the gas-phase pyrolysis of cellulose-and kraft lignin-derived volatile matter. *Ind. Engg Chem. Prod Res Develop.* 22 (2):366–75.

Antal, M. 1985. A review of the vapor phase pyrolysis of biomass derived volatile matter. *Fundam Thermochem. Biomass Convers.* 511–37.

Boroson, M., J. Howard, J. Longwell, and W. Peters. 1989. Product yields and kinetics from the vapor phase cracking of wood pyrolysis tars. *AIChE J.* 35 (1):120–28. doi:10.1002/aic.690350113.

Borujerdi, P., and B. Shotorban. 2022. Pyrolysis and combustion characteristics of leaf-like fuel under convection and radiation heating. *Combust Sci. Technol* 194 (12) : 2558–2579.

Borujerdi, P. R., B. Shotorban, and S. Mahalingam. 2020. A computational study of burning of vertically oriented leaves with various fuel moisture contents by upward convective heating. *Fuel* 276:118030. doi:10.1016/j.fuel.2020.118030.

Bryden, K. M., and M. J. Hagge. 2003. Modeling the combined impact of moisture and char shrinkage on the pyrolysis of a biomass particle. *Fuel* 82 (13):1633–44. doi:10.1016/S0016-2361(03)00108-X.

Bryden, K. M., K. W. Ragland, and C. J. Rutland. 2002. Modeling thermally thick pyrolysis of wood. *Biomass Bioenergy.* 22 (1):41–53. doi:10.1016/S0961-9534(01)00060-5.

Burrows, N. 2001. Flame residence times and rates of weight loss of eucalypt forest fuel particles. *Int J. Wildland Fire* 10 (2):137–43. doi:10.1071/WF01005.

Datta, B. N. 2010. *Numerical linear algebra and applications*. 2nd ed, Vol. 116. Philadelphia, PA, USA: SIAMa.

Di Blasi, C. 2008. Modeling chemical and physical processes of wood and biomass pyrolysis. *Prog Energy Combust Sci.* 34 (1):47–90. doi:10.1016/j.pecs.2006.12.001.

Evans, R., and T. Milne. 1987. Molecular characterization of the pyrolysis of biomass. *Energy Fuels.* 1 (2):123–37. doi:10.1021/ef00002a001.

Gallacher, J. R. 2016. The influence of season, heating mode and slope angle on wildland fire behavior. PhD dissertation., Provo, UT: Brigham Young University.

Grishin, A. M. 1997. *Mathematical modeling of forest fires and new methods of fighting them*. Publishing house of the Tomsk state university.

Grosshandler, W. L. 1993. *Radcal: A narrow band model for radiation*. Gaithersburg, MD, USA: Calculations in a Combustion Environment, NIST Technical Note 1402.

Koufopanos, C., A. Lucchesi, and G. Maschio. 1989. Kinetic modelling of the pyrolysis of biomass and biomass components. *Canad J. Chem Engg.* 67 (1):75–84. doi:10.1002/cjce.5450670111.

Lautenberger, C. 2014. *Gpyro–a generalized pyrolysis model for combustible solids*. Berkeley, CA: Technical Reference Version 0.8, Reax Engineering Inc.

Lee, D., H. Yang, R. Yan, and D. Liang. 2007. Prediction of gaseous products from biomass pyrolysis through combined kinetic and thermodynamic simulations. *Fuel* 86 (3):410–17. doi:10.1016/j.fuel.2006.07.020.

Leroy, V., E. Leoni, and P. Santoni. 2008. Reduced mechanism for the combustion of evolved gases in forest fires. *Combust. Flame* 154 (3):410–33. doi:10.1016/j.combustflame.2008.04.014.

Matt, F. J., M. A. Dietenberger, and D. R. Weise. 2020. *Summative and ultimate analysis of live leaves from southern us forest plants for use in fire modeling* 34 (4): 4703–4720.

McAllister, S., and M. Finney. 2017. Autoignition of wood under combined convective and radiative heating. *Proceed. Combust Inst.* 36 (2):3073–80. doi:10.1016/j.proci.2016.06.110.

McGrattan, K., S. Hostikka, R. McDermott, J. Floyd, C. Weinschenk, and K. Overholt. 2013. *Fire dynamics simulator technical reference guide volume 1: Mathematical model*. Gaithersbug, MD, USA: Special Publication 1018-6, U.S. Department of Commerce, National Institute of Standards and Technology.

Mell, W., A. Maranghides, R. McDermott, and S. Manzello. 2009a. Numerical simulation and experiments of burning douglas fir trees. *Combust. Flame* 156 (10):2023–41. doi:10.1016/j.combustflame.2009.06.015.

Mell, W., A. Maranghides, R. McDermott, and S. L. Manzello. 2009b. Numerical simulation and experiments of burning douglas fir trees. *Combust. Flame* 156 (10):2023–41. doi:10.1016/j.combustflame.2009.06.015.

Miller, R., and J. Bellan. 1997. A generalized biomass pyrolysis model based on superimposed cellulose, hemicelluloseand liqnin kinetics. *Combust Sci. Technol.* 126 (1–6):97–137. doi:10.1080/00102209708935670.

Morvan, D., and J. Dupuy. 2001. Modeling of fire spread through a forest fuel bed using a multiphase formulation. *Combust. Flame* 127 (1–2):1981–94. doi:10.1016/S0010-2180(01)00302-9.

Morvan, D., M. Larini, J. Dupuy, P. Fernandes, A. Miranda, J. Andre, O. Séro-Guillaume, D. Calogine, and P. Cuiñas. 2004. *Behaviour modelling of wildland fires: A state of the art. EUFIRELAB: Euro-Mediterranean wildland fire laboratory, a wall-less laboratory for wildland fire sciences and technologies in the Euro-Mediterranean region*. Warszawa, Poland: Reports, EU FIRE LAB.

Ni, M., D. Leung, M. Leung, and K. Sumathy. 2006. An overview of hydrogen production from biomass. *Fuel Process. Technol.* 87 (5):461–72. doi:10.1016/j.fuproc.2005.11.003.

Peters, N., and R. Kee. 1987. The computation of stretched laminar methane-air diffusion flames using a reduced four-step mechanism. *Combust. Flame* 68 (1):17–29. doi:10.1016/0010-2180(87)90062-9.

Pickett, B. M., 2008. Effects of moisture on combustion of live wildland forest fuels. PhD dissertation., Provo, UT: Brigham Young University.

Pickett, B. M., C. Isackson, R. Wunder, T. H. Fletcher, B. W. Butler, and D. R. Weise. 2010. Experimental measurements during combustion of moist individual foliage samples. *Int J. Wildland Fire* 19 (2):153–62.

Prince, D. R., 2014. Measurement and modeling of fire behavior in leaves and sparse shrubs. PhD dissertation., Provo, UT: Brigham Young University.

Prince, D. R., and T. H. Fletcher. 2014. Differences in burning behavior of live and dead leaves, part 1: Measurements. *Combust Sci. Technol.* 186 (12):1844–57. doi:10.1080/00102202.2014.923412.

Ritchie, S., K. Steckler, A. Hamins, T. Cleary, J. Yang, and T. Kashiwagi. 1997. The effect of sample size on the heat release rate of charring materials. *Fire Saf Sci.* 5:177–88. doi:10.3801/IAFSS.FSS.5-177.

Safdari, M. S., 2018. Characterization of pyrolysis products from fast pyrolysis of live and dead vegetation. PhD dissertation., Provo, UT.

Safdari, M., E. Amini, D. Weise, and T. Fletcher. 2020. Comparison of pyrolysis of live wildland fuels heated by radiation vs. convection. *Fuel* 268:117342. doi:10.1016/j.fuel.2020.117342.

Safdari, M. S., M. Rahmati, E. Amini, J. E. Howarth, J. P. Berryhill, M. Dietenberger, D. R. Weise, and T. H. Fletcher. 2018. Characterization of pyrolysis products from fast pyrolysis of live and dead vegetation native to the southern United States. *Fuel* 229:151–66. doi:10.1016/j.fuel.2018.04.166.

Scott, D., J. Piskorz, and D. Radlein. 1985. Liquid products from the continuous flash pyrolysis of biomass. *Indus Engg. Chem Process Des Develop.* 24 (3):581–88. doi:10.1021/i200030a011.

Sheng, C., and J. Azevedo. 2002. Modeling biomass devolatilization using the chemical percolation devolatilization model for the main components. *Proceed Combust Inst.* 29 (1):407–14. doi:10.1016/S1540-7489(02)80054-2.

Shotorban, B., B. L. Yashwanth, S. Mahalingam, and D. J. Haring. 2018. An investigation of pyrolysis and ignition of moist leaf-like fuel subject to convective heating. *Combust. Flame* 190:25–35. doi:10.1016/j.combustflame.2017.11.008.

Smith, G., D. Golden, M. Frenklach, N. Moriarty, B. Eiteneer, M. Goldenberg, C. Bowman, R. Hanson, S. Song, W. Gardiner Jr, et al. 2000. Gri-mech. *Gas Res. Inst*. http://www.me.berkeley.edu/grimech

Tihay, V., P. A. Santoni, A. Simeoni, J. P. Garo, and J. P. Vantelon. 2009. Skeletal and global mechanisms for the combustion of gases released by crushed forest fuels. *Combust. Flame* 156 (8):1565–75. doi:10.1016/j.combustflame.2009.05.004.

Turns, S. 1996. *Introduction to combustion*, Vol. 287. New York, NY, USA: McGraw-Hill Companies.

Wagenaar, B., W. Prins, and W. van Swaaij. 1993. Flash pyrolysis kinetics of pine wood. *Fuel Process. Technol.* 36 (1–3):291–98. doi:10.1016/0378-3820(93)90039-7.

Wilken, G. C. 1967. Snow accumulation in a manzanita brush field in the sierra nevada. *Water Resour. Res.* 3 (2):409–22. doi:10.1029/WR003i002p00409.

Wurzenberger, J., S. Wallner, H. Raupenstrauch, and J. Khinast. 2002. Thermal conversion of biomass: Comprehensive reactor and particle modeling. *AIChE J.* 48 (10):2398–411. doi:10.1002/aic.690481029.

Yashwanth, B., B. Shotorban, S. Mahalingam, C. Lautenberger, and D. Weise. 2016. A numerical investigation of the influence of radiation and moisture content on pyrolysis and ignition of a leaf-like fuel element. *Combust. Flame* 163:301–16. doi:10.1016/j.combustflame.2015.10.006.

Zhou, X., and S. Mahalingam. 2001. Evaluation of reduced mechanism for modeling combustion of pyrolysis gas in wildland fire. *Combust Sci. Technol.* 171 (1):39–70. doi:10.1080/00102200108907858.

Zhou, X., and J. Pereira. 1998. Comparison of four combustion models for simulating the premixed combustion in inert porous media. *Fire Mater.* 22 (5):187–97. doi:10.1002/(SICI)1099-1018(199809/10)22:5<187:AID-FAM652>3.0.CO;2-T.

Zhou, X., D. Weise, and S. Mahalingam. 2005. Experimental measurements and numerical modeling of marginal burning in live chaparral fuel beds. *Proceed Combust. Inst.* 30 (2):2287–94. doi:10.1016/j.proci.2004.08.022.